A Deep SCUBA-2 450µm Survey of the GOODS-N and GOODS-S Fields

Ariana Blair

Advisor: Prof. Amy Barger

University of Wisconsin - Madison

May 4, 2020

1 Introduction

Submillimeter galaxies (SMGs) are some of the most powerful star-forming galaxies in the universe. The use of deep imaging with the Submillimeter Common-User Bolometer Array (SCUBA: Holland et al. 1999) on the 15m James Clerk Maxwell Telescope (JCMT) brought these galaxies into view for astronomers. They found these newly discovered galaxies to be distant, but dusty and extremely luminous (e.g. Smail et al. 1997; Barger et al. 1998; Younger et al. 2007), indicating high star formation rates (SFRs). Because of this, they are significant contributors to the star formation history (Chapman et al. 2005; Casey et al. 2013; Barger et al. 2014; Cowie et al. 2017; Lim et al. 2020), making them critical in understanding galactic evolution.

Prior to submillimeter studies and the discovery of SMGs, optical and ultra-violet (UV) studies were primarily used. With the advancement of infrared (IR) telescopes, we saw another layer in star formation and galactic evolution. When looking at the star formation currently happening in a galaxy, UV observations show the output of the young, hot stars currently in a galaxy. Because of their short life spans, they make good estimates for current SFRs. However, dust within a galaxy absorbs that intense UV radiation, heating the dust to around 30-60K. The warm dust radiates in the FIR, peaking around 100µm, and giving the galaxy a characteristic dust spectrum. The flux density of these longer wavelengths — the Rayleigh-Jeans regime — is well-described by a modified blackbody, also known as a graybody, shown as

$$S(\nu, T) \propto \nu^{2+\beta}$$

where ν is the frequency, T is a given temperature, and the flux density is in units of Jy. β describes the spectral emissivity index and typically found between 1-2 for starburst galaxies like SMGs (Hildebrand 1983; Dunne et al. 2001; Draine 2006).

While this applies to the local universe, it changes as we move to higher cosmological redshifts. All emitted light from a galaxy is shifted to longer wavelengths, placing the peak of a galaxy's dust spectrum clearly in the submillimeter (200-1000µm) around z=1-3. Because the submillimeter is probing that redshifted dust spectrum, we find highly luminous and star-forming galaxies, similar to lower redshift Ultra Luminous Infrared Galaxies (ULIRGs) like Arp220. The UV light produced by the young stars in these galaxies creates a luminous dust spectrum. Consequentially, the galaxy can become obscured and sometimes invisible to traditional UV-optical observation because of the dust absorption, making submillimeter studies crucial in uncovering these veiled galaxies.

Additionally, optical and radio wavelengths dim according to the inverse square law, making them far fainter and more difficult to observe at high redshift. Submillimeter, on the other hand, does not suffer those effects as shown in Figure 1. Because of the shape and steepness of the dust spectrum associated with highly star forming galaxies, as that spectral energy distribution (SED) is redshifted, we actually start probing the peak of the dust spectrum, maintaining or even increasing the fluxes of the sources, rather than dimming it (Blain et al. 2002). This gives submillimeter astronomy a massive advantage when searching for high redshift sources.

However, some challenges still persist with submillimeter astronomy, primarily with the angular resolution and confusion limits of current submillimeter instruments. Ground-based instruments must observe through narrow atmospheric windows along with strict weather requirements. Because of observation difficulties, 850µm has been one of the most accessible wavelengths for submillimeter studies (e.g. Barger et al. 1998; Coppin et al. 2006; Chen et al. 2013a; Barger et al. 2014; Cowie et al. 2017, 2018). These observations probe galaxies from z=1-6 with the majority sitting around z=2-3 (Barger et al. 2000; Chapman et al. 2003; Chapman et al. 2005; Casey et al. 2013; Dunlop 2016; Cowie et al. 2017). The major drawback from 850µm is its poorer angular resolution, with a beam size of $14''$ on SCUBA-2

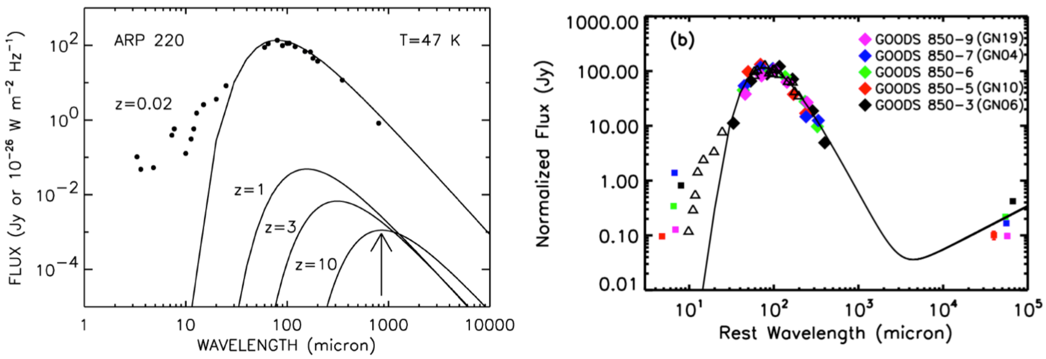

Figure 1 Left: The ULIRG Arp220 is (Klaas et al. 1997; Rigopoulou et al. 1996) is well-represented in the FIR/submillimeter by a graybody normalized at 800µm. This graybody has been redshifted to z=1, 3, 10 with the arrow pointing to 850µm. As the peak of the dust spectrum is redshifted, we are probing closer to it while not experiencing significant dimming. Right: Multiple SCUBA sources in the GOODS-N normalized and plotted against Arp220 (triangles) and a greybody curve, showing the similarity among SCUBA galaxies. Figure from Barger et al. (2012).

(Holland et al. 2013). While this is impressive for submillimeter instruments, it still results in unresolved galaxies and source blending.

To combat this poor resolution, astronomers have looks to other wavelengths with better resolution. SMGs often have faint or no optical counterpart, so optical observations cannot reliably identify true counterparts to SMGs. Fortunately, centimeter wavelength observations have subarcsecond positional accuracy and resolution that can aid in identifying counterparts to SMGs (Barger et al. 2000). The Karl G. Jansky Very Large Array (VLA) is the most common telescope used for radio continuum observations (5-20cm). Furthermore, there is also a tight correlation between infrared dust and radio continuum emissions (Helou et al. 1985; Condon et al. 1991). Although this linear correlation is not well understood, both submillimeter and radio observations probe recent star formation in a galaxy, likely resulting in the relation we see (Condon 1992). We can use this relation as a redshift estimate, which is especially important for SMGs as it can be challenging to find a spectroscopic redshift.

In addition to radio imaging, advancements have been made in submillimeter imaging. The Submillimeter Array (SMA; Ho et al. 2004) and more recently the Atacama Larger Millimeter/Submillimeter Array (ALMA) are both powerful imagers capable of identifying that some submillimeter sources are in fact multiple sources that are lost in the poorer resolution of single-dish submillimeter telescopes (e.g. Wang et al. 2011; Hodge et al. 2013; Chen et al. 2013). Unfortunately, because of their small field of view, they are not viable options for finding large samples of submillimeter sources.

Single-dish submillimeter telescopes like JCMT are much faster at finding submillimeter sources. A major advantage to using SCUBA-2 for submillimeter observations is its ability to collect data at 450µm and 850µm simultaneously, making it extremely efficient. Having both 450µmm and 850µm flux measurements also allows us to build a SED. Because these wavelengths straddle opposing sides of the dust spectrum, we can better construct the necessary SEDs with the measured fluxes.

As mentioned earlier, studies with the 850µm observations have been far more common, but there is a great advantage to using the 450µm observations instead. It has a far greater angular resolution (7.5″), which is critical when identifying counterparts, and we are staying within the submillimeter instead of resorting to other wavelengths. Along with SCUBA-2's wide field of view, it is far superior to other instruments in its class like 500µm from *Herschel* (Pilbratt et al. 2010) (35″).

While 450µm data is a great option for SMGs studies, its strict weather requirements make obtaining data challenging. Even with SCUBA-2 located at one of the best places on Earth for submillimeter astronomy, only around 15% of the year is there low enough water vapor for 450µm observations. Up until recently, 450µm studies have often been too minimal and shallow for extensive galaxy surveys. Pushing to deeper depth allows us to more completely probe the 450µm population to understand possible differences between the 850µm and 450µm populations. While it seems as though most of their physical properties are similar, 450μm sources occupy a slightly lower redshift range (z=1-2) and are warmer and dustier than 850μm sources (Casey et al. 2013; Roseboom et al. 2013).

For this thesis, I have worked on providing a deeper study of 450μm sources, where we have compiled several years worth of observations of the GOODS-N/S, achieving central rms of 1.45 mJy for the GOODS-N and 2.64 mJy for the GOODS-S and identifying 91 and 21 sources respectively at $>4\sigma$. We match these sources to ultradeep VLA 20 cm data (GOODS-N) and ALMA 850μm data (GOODS-S) to gauge the 450μm positional accuracy and apply corrections to our positions. Using the 850μm/ 450μm vs redshift and 20cm/ 850μm vs redshift, we make cuts for possible high redshift candidates in the GOODS-N. We then use 450μm/850μm vs 850μm/20 cm to check our high redshift candidates.

2 Observations

2.1 Fields

Our main goals of this project were to create catalogs of 450μm sources and search for counterparts in 850μm and 20cm imaging in order to better understand important properties such as star formation and redshift. In order to achieve these goals, we needed to choose fields with deep multiwavelength imaging. With this in mind, we chose the GOODS-N and GOODS-S. These fields are extremely well-studied in multiple wavelengths, making them excellent for our study. Our chosen regions have a combination of deep ground-based coverage in the optical (B through z) from HST surveys using the ACS (Giavalisco et al. 2004) and two NIR bands from the HST CANDELS survey using the WFC3 (Grogin et al. 2011; Koekemoer et al. 2011). There is also available deep MIR data from the *Spitzer* 70μm survey using MIPS, which comes with 24μm and 160μm data. *Herschel* surveys using PACS and SPIRE also provide some of the deepest FIR imaging (Elbaz et al. 2011; Lutz et al. 2011). For the GOODS-N specifically, there are hundreds of hours of 20cm observations resulting in 1σ sensitivity of 2.2 µJy (Barger et al. 2012, 2014, 2017; Owen 2018) which we take advantage of in our study. Finally, the GOODS fields have by far the deepest X-ray images with *Chandra* obtaining a 7 Ms and 2 Ms images of the *Chandra* Deep Field - South (CDF-S; Luo et al. 2017) and *Chandra* Deep Field - North (CDF-N; Alexander et al. 2003) respectively. On top of this extensive multiwavelength study, the GOODS fields both have spectroscopic and photometric redshifts for thousands of galaxies (e.g. Popesso et al. 2009; Hsu et al. 2014; Skelton et al 2014; Barger et al. 2019). Our observations with SCUBA-2 cover nearly the entire GOODS area and lie in the most sensitive regions of the *Chandra* images.

2.2 Observation Runs

Our primary instrument for studying SMGs is the Submillimeter Common-User Bolometer Array 2 (SCUBA-2; Holland et al. 2013), mounted on the 15m James Clark Maxwell Telescope on Mauna Kea in Hawai'i. SCUBA-2 operates and produces images for 850µm and 450µm simultaneously, making it extremely efficient for multiwavelength studies (e.g. Casey et al. 2013; Barger et al. 2014; Cowie et al. 2017, 2018; Wang et al. 2017; Lim et al. 2020). Its field of view of 50 arcsec^2 allows us to image large sections of the night sky with some of the best angular resolution from the ground.

We have been observing the GOODS-N/S since SCUBA-2 became operational. With nearly a decade of observations, we have extremely deep images of these fields, allowing us to probe faint SMGs that are underrepresented in studies. Furthermore, even though SCUBA-2 has excellent angular resolution for its class of instrument, it is unable to resolve these sources. We need our imaging to be as deep as possible to reduce noise and detect faint SMGs.

When scanning the night sky, SCUBA-2 uses different patterns in order to achieve varying sensitivity and depths. For our observations we use the CV Daisy and PONG-900 scanning

Table 1. SCUBA-2 GOODS-N/S 450µm Observations

Field	Weather Band	Scan Pattern.	Exposure (Hr)
GOODS-N	1	CV Daisy	80.08
	2	CV Daisy	25.0
	3	CV Daisy	4.5
	1	PONG-900	14.0
	2	PONG-900	88.24
	3	PONG-900	25.34
GOODS-S	1	CV Daisy	30.76
	2	CV Daisy	45.0
	3	CV Daisy	5.5
	1	PONG-900	6.0
	2	PONG-900	48.82
	3	PONG-900	14.72

patterns. Using the CV Daisy imaging would give us excellent depth in the center of the image, but the edges are more noisy. In contrast, the PONG-900 scan pattern covers a wider view. By combining these images in the reduction process, we have better depth through the entire image. However, the central area of the image is always the deepest as shown in Figure 2.

As seen in Table 1, we have many, many, many hours of observation on these two fields. While this is obviously very time consuming, it is the only way to properly study these fields. Because SCUBA-2 is ground-based, we have to compete with the water vapor in the atmosphere, which is opaque to most submillimeter wavelengths. Small windows exist at 850µm and 450µm which is why they are the wavelengths observed with SCUBA-2. Even observing through these windows, there is still enough noise that makes a single scan useless when studying SMGs.

Because of the moisture in the atmosphere, our observations have strict weather requirements to further reduce the noise. In Table 1 the different scans are further denoted by the

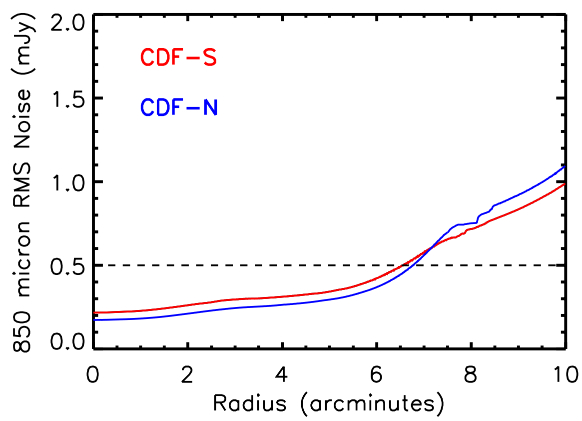

Figure 2 The 850µm RMS noise for the CDF-N/S. The noise is the lowest in the center and increase as you move out to the edges.

weather band that they were observed in. These bands are determined by the water vapor in the air, with Band 1 having the lowest, making it the best conditions to observe in. For our observations, 850µm can be observed up to Band 3, but Band 2 or lower is preferred. On the other hand, 450µm has even tighter requirements due to its atmospheric window being poorer, so it is mostly viable in Band 1.

Because of 450µm observing requirements, it has long gone understudied. Within the past couple of years, we had excellent weather during our runs, giving us plenty of 450µm data to use for this study. An advantage of studying SMGs with 450µm data is its greater angular resolution, so we can find accurate positions of the sources to do multiwavelength studies.

2.3 Catalogs

Along with our SCUBA-2 observations of the GOODS-N/S, we also use catalogs from Cowie et al. (2018) (ALMA 850µm) , Cowie et al. (2017) (SMA 850µm) and Owen (2018) (VLA 20cm). These catalogs are used to test the positions of our 450µm sources through a matching process. We also use the fluxes and redshifts of the counterparts in our later analysis.

3 Data Reduction

One of the most time intensive, yet crucial part of our studies is data reduction. We have to take the hours and many gigabytes of observations and combine them into a single image. We compile all of our reduced images into one master image. Stacking the same image again and again gives us the necessary depth and noise reduction to effectively study these galaxies.

These reductions can be complicated, so I had to be trained in order to understand how the telescope works, how our observations are done, and how to reduce the raw data. To begin this training, I traveled to JCMT in order to have hands-on experience working with the telescope and data. I observed there for three nights at the end of January 2018, gaining valuable knowledge about the scientific process. These nights in particular ended up being some of our most successful nights in collecting 450µm data, so it was fitting for me to work with the data I helped collect.

I will not going into great detail on the specifics of data reduction as it is a long and complex process. As mentioned earlier, we use the CV Daisy and PONG-900 scan patterns in order to get the best image quality and depth. We download the raw data from the CADC website along with a few calibrators. The reduction process that we follow is described in Chen et al. (2013b), and this particular reduction process is detailed in Cowie et al. (2017).

As a brief overview, we reduce the data using the Dynamic Iterative Map Maker (DIMM) which applies an assortment of corrections to the common mode signal, astronomical signal, and white noise, all while correcting any extinction. The maps comes in four pieces that need to be combined, so wee use the MOSAIC_JCMT_IMAGES recipe in the Pipeline for Combining and Analyzing Reduced Data (PICARD; Jenness et al. 2008) to merge the pieces in order to form the images. We then apply a calibration to the fluxes using Flux Conversion Factors (FCF) determined by our calibrator images. Each night and field has a different number that fluctuates with the particular calibrator and the particular weather conditions at that time.

The final step is to run a matched-filter S/N (signal to noise) over the images. This fits a single Gaussian point spread function (PSF), centered over every pixel in the map. A background suppression filter is applied to further reduce the noise, and we have the completed image for that night. Each individual observation is merged to create a single image of the field that we use in our analysis.

4 Data Analysis

4.1 Source Extraction

With our images fully reduced and all observations unified into a single main image of each field, we can search them for our sources. I was given a simple python source extraction code written by a collaborator, and I used that code on both the GOODS-N and GOODS-S 450µm images. An advantage to the S/N maps that we make is that each pixel value is the flux at that position in the sky, making extraction simple. I set the detection criteria to be $>4\sigma$ in order to have near-definite source detections. With this as the main requirement, we found 91 sources in the GOODS-N and and 21 in the GOODS-S, with central noise values of 1.45 mJy/beam and 2.64 mJy/beam respectively.

Due to the ease of flux extraction with SCUBA-2's images and the excellent positional accuracy of ALMA and the VLA, we also worked backwards. We use the VLA (GOODS-N) and ALMA (GOODS-S) positions to extract 850µm and 450µm fluxes. We can then bypass the lower resolution of SCUBA-2 and image depth issues. Using this method, we found that most of the VLA and ALMA sources had a positive fluxes at their positions. However, in subsequent sections, we will utilize the 450μm sample discussed above.

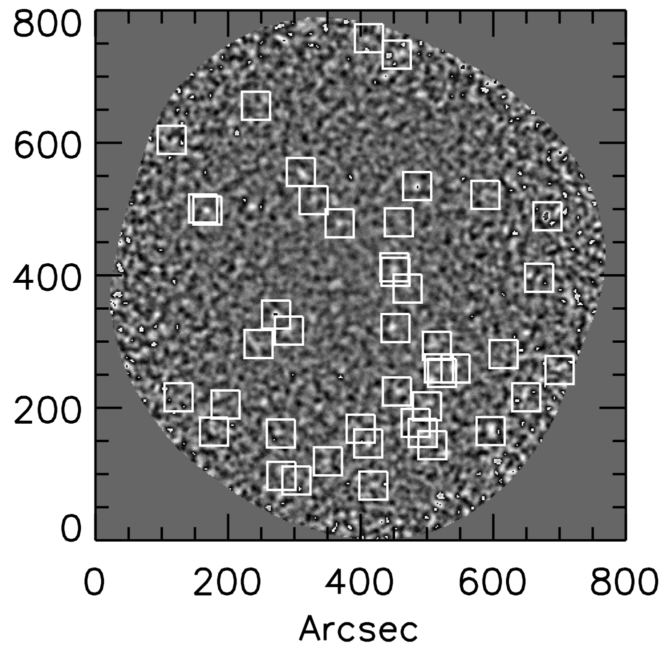

Figure 3 SCUBA-2 450μm image of the GOODS-S. The white squares indicate the ALMA sources >2.25mJy.

4.2 Catalog Matching

After our primary source extraction directly from the 450μm SCUBA-2 images, we compared our sources to the 20cm catalog in Owen (2018) and 850μm catalog in Cowie et al. (2018). The VLA and ALMA both have greater positional accuracy than SCUBA-2, so we perform a matching process (VLA for the GOODS-N, ALMA for the GOODS-S) to gauge the position of our sources as well as identify correct counterparts for our later analysis. For the GOODS-N we found that out of the 91 sources, 84 were within the 20cm observations. When we applied a $4''$ restriction to the counterparts, we found 65 with a 20cm counterpart. We did the same with the 14 sources in the GOODS-S. When the same $4''$ restriction was applied, we found 14 with a 850μm counterpart. Comparing our source positions to these catalogs gave us positional corrections, which we applied to each of our sources.

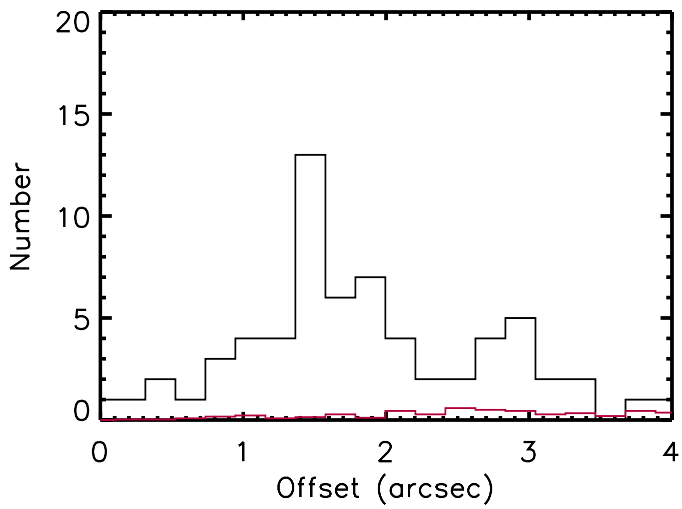

Figure 4 Offsets between the 65 SCUBA-2 450µm central positions and the radio counterpart positions within 4″. The red curve shows the histogram of offsets that would be expected between the positions of a random distribution of 450µm sources and the radio positions for counterparts within 4″, based on 64 simulations.

5 Discussion

5.1 Flux Ratios

Since most SMGs are optically faint, obtaining accurate redshifts is challenging. Positional accuracy is also a problem as we need a precise position to make sure the galaxy's light will go through the typically 1″ wide slit of the mask and reach the spectrograph. To work around these problems, we can use different flux ratios in the submillimeter and radio to estimate redshifts. For submillimeter flux ratios, it has been found that the SEDs of SMGs seem to be relatively similar (Barger et al. 2012; Cunha et al. 2015), meaning we can use fluxes that straddle the peaks of the SED's dust spectrum to give us reasonable redshift estimates. We can similarly use radio-submillimeter flux ratios to estimate redshifts for galaxies. As mentioned in the beginning, there is a tight correlation between the radio and submillimeter fluxes.

Something important we can select when looking at the flux ratios of sources are high redshift candidates. As mentioned previously, SMGs are often highly star-forming because the submillimeter probes the peak of a redshifted dust spectrum. There have been a select number of very luminous millimeter galaxies measured to have redshifts around z$\sim$6 (Strandet et al. 2016). This pushes what we know about the hierarchical model of galaxy formation as bright, massively star-forming submillimeter galaxies may be common at that redshift. Finding more of these high redshift submillimeter galaxies will help us trace the star formation history of the universe and better understand how galaxies formed in the early universe.

Because the GOODS-N has observations in 450µm, 850µm, and 20cm, we can use flux ratios to find redshift estimates and make cuts for those at high redshifts. Starting with 20cm/850µm vs redshift, we see a good correlation to make our redshift cuts. Those marked in blue are z>3 and those marked in red are z>4. These are spectroscopically confirmed. Any black point on the far left has not been spectroscopically confirmed. Based on the flux ratios of the sources, we are able to make cuts for possible high redshift sources. Those marked in gold on the far left in Figure 5 make that cut.

To make another selection, we plotted 450µm/850µm vs redshift in order to get another cut. We again see a good correlation so we can make cuts like before. Similar to the other plot in Figure 5, points marked in blue are z>3 and those marked in red are z>4. With these redshifts and their associated flux ratios, we make a cut below the highest red point and mark those with a possible high redshift in green.

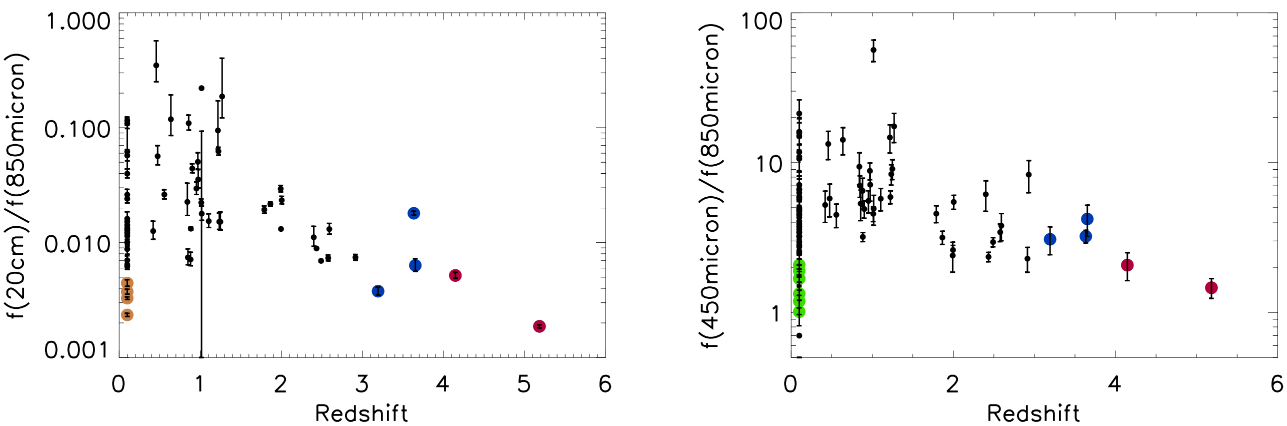

Figure 5 Left:GOODS-N 20cm/850μm vs redshift. Gold indicates possible high redshift sources. Right: GOODS-N 450μm/850μm vs redshift. Green indicate possible high redshift sources.

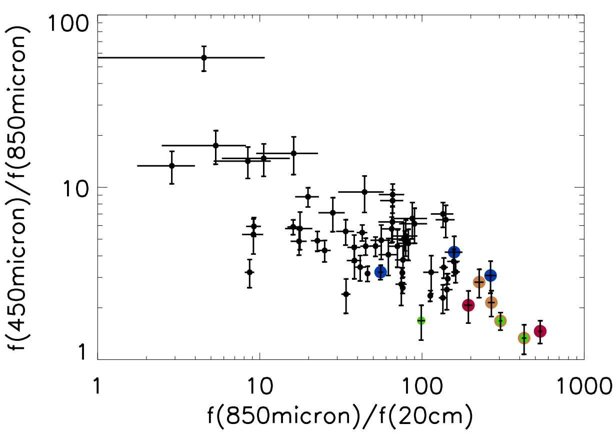

Figure 6 GOODS-N 450μm/850μm vs 850μm/20cm. Gold and green points indicate high redshift sources.

As a final determination for possible high redshift sources, we then plotted 450μm/850μm vs 850μm/20cm. This plot differs by removing redshift from the equation entirely. Because of the correlations between the FIR and the radio, we can also use this plot to identify and cross-check our cuts from the previous plots. With the same notation as the prior plots, we see there is some overlap with the gold and green sources from Figure 5 in Figure 6. We did lose some green sources because they were not in the radio observation area. Those that do overlap are ringed in gold with a green center. These sources sit close to the red points, indicating that they likely are high redshift sources.

6 Summary and Future Work

6.1 Summary

This senior thesis looked to utilize our deep SCUBA-2 450µm observations of the two GOODS fields. We identified 91 and 21 sources at $>4\sigma$ in the GOODS-N and GOODS-S respectively. We used available 20cm VLA and 850µm ALMA catalogs to identify counterparts within a $4''$ radius around each SCUBA-2 source. Of the 84 in the GOODS-N that were within the 20cm observations, 65 had counterparts, and 14 had 850µm counterpart in the GOODS-S. Comparing the positions gave us corrections to our SCUBA-2 positions.

Then, working backwards, we took the 20cm positions from their catalogs and extracted the 850µm and 450µm fluxes from our SCUBA-2 images of the GOODS-N. We similarly took the 850µm positions in the GOODS-S and extracted the 450µm flux. However, we decided to utilize the 450µm sample and the identified counterparts.

Because of the tight correlation of submillimeter-radio ratio and having two submillimeter fluxes that straddle the dust spectrum, we can make redshift estimations and cuts for high redshift candidates. Since the GOODS-N has observations in all three wavelengths, we created flux ratios vs redshift for our 450 micron sample. We used the fluxes extracted from our 850µm SCUBA-2 image of the GOODS-N and from the identified counterparts from the 20cm catalog. We plotted 450µm/850µm vs redshift and 850µm/20cm vs redshift. Comparing the points without spectroscopic redshifts to those with, we could make cuts for sources with potential z>4.

With those cuts made, we plotted 450µm/850µm vs 850µm/20cm. The two methods did find some of the same candidates, shown in Figure 3. We also lost some sources due to needing to be in the 20cm observations. In total, we ended up with a total of 5 possible high redshift candidates.

6.2 Future Work

Moving forward from what has been detailed in this thesis, there is much we can still do with this data. We need to calculate the current star formation rates for our sources through their SEDs. This is critical in trying to understand how SMGs contribute overall to the universe's star formation history, especially at high redshifts.

We also will continue observing these fields with SCUBA-2. More observations will further reduce noise in our images and make it possible for us to detect fainter sources, giving us a more complete look at the submillimeter population.

Finally, determining redshifts for more SMGs is important because they are key to determining many physical properties of SMGs, including their physical size, luminosities, and stellar masses. Obtaining optical/NIR redshifts with the Keck telescopes would be ideal, but because of SMGs optical faintness, we often need to use other methods such as millimeter spectral scans with ALMA and NOEMA. These observations are very time intensive, making obtaining spectroscopic redshift for large samples hard, so we will use photometric redshifts based on full SEDs (UV to FIR). These rely on the extensive multiwavelength observations mentioned earlier in the GOODS fields. For optically faint sources, this will rely mostly on the dust peak in the FIR/submillimeter. Determining more redshifts will also help us collect more high redshift SMGs and understand galaxy formation and star formation in the early universe.

References

Alexander, D. M., Bauer, F. E., Brandt, W. N., et al. 2003, AJ, 126, 539
Barger, A. J., Cowie, L. L., Bauer, F. E., et al. 2019, ApJ, 887, 23
Barger, A. J., Cowie, L. L., Chen, C.-C., et al. 2014, ApJ, 784, 9
Barger, A. J., Cowie, L. L., Owen, F. N., Hsu, L.-Y., & Wang, W.-H. 2017,ApJ, 835, 95
Barger, A. J., Cowie, L. L., Richards, E. A. 2000, AJ, 119, 2092
Barger, A. J., Cowie, L. L., Sanders, D. B., et al. 1998, Natur, 394, 248
Barger, A. J., Wang, W.-H., Cowie, L. L., et al. 2012, ApJ, 761, 89
Blain, A. W., Smail, I., Ivison, R. J., Kneib, J.-P., & Frayer, D. T. 2002, PhR, 369, 111
Casey, C. M., Chen, C.-C., Cowie, L. L., et al. 2013, MNRAS, 436, 1919
Chapman, S. C., Barger, A. J., Cowie, L. L., et al. 2003, ApJ, 585, 57
Chapman, S. C., Blain, A. W., Smail, I., Ivison, R. J. 2005, ApJ, 622, 772
Chen, C.-C., Cowie, L. L., Barger, A. J., et al. 2013a, ApJ, 762, 81
Chen, C.-C., Cowie, L. L., Barger, A. J., et al. 2013b, ApJ, 776, 131
Condon, J. J. Anderson, M. L., & Helou, G. 1991, ApJ, 376, 95.
Cowie, L. L., Barger, A. J., Hsu, L.-Y., et al. 2017, ApJ, 837, 139
Cowie, L. L., Gonz alez-L opez, J., Barger, A. J., et al. 2018, ApJ, 865, 106
da Cunha, E., Walter, F., Smail, I. R., et al. 2015, ApJ, 806, 110
Dunlop, J. S., McLure, R. J., Biggs, A. D., et al. 2017, MNRAS, 466, 861
Dunne, L. & Eales, S. A. 2001, MNRAS, 327, 697
Draine, B. T. 2006, ApJ, 636, 1114
Elbaz, D., Dickinson, M., Hwang, H. S., et al. 2011, AA, 533, A119
Giavalisco, M., Dickinson, M., Ferguson, H. C., et al. 2004, ApJL, 600, L93
Grogin, N. A., Kocevski, D. D., Faber, S. M., et al. 2011, ApJS, 197, 35
Helou, G., Soifer, B. T., & Rowan-Robinson, M. 1985, ApJ, 298, L7.
Hildebrand, R. H. 1983, QJRAS, 24, 267
Ho, P. T. P., Moran, J. M., & Lo, K. Y. 2004, ApJL, 616, L1
Hodge, J. A., Karim, A., Smail, I., et al. 2013, ApJ, 768, 91
Holland, W. S., Bintley, D., Chapin, E. L., et al. 2013, MNRAS, 430, 2513
Hsu, L.-T., Salvato, M., Nandra, K., et al. 2014, ApJ, 796, 60
Klaas, U., Haas, M., Heinrichsen, I., & Schulz, B. 1997, A&A, 325, L21.
Koekemoer, A. M., Faber, S. M., Ferguson, H. C., et al. 2011, ApJS, 197, 36
Lim, C.-F., Wang, W.-H., Smail, I., et al. 2020, ApJ, 889, 80
Luo, B., Brandt, W. N., Xue, Y. Q., et al. 2017, ApJS, 228, 2
Lutz, D., Poglitsch, A., Altieri, B., et al. 2011, A&A, 532, A90
Owen, F. N. 2018, ApJS, 235, 34
Pilbratt, G. L., Riedinger, J. R., Passvogel, T., et al. 2010. AA, 518, L1
Popesso, P., Dickinson, M., Nonino, M., et al. 2009, AA, 494, 443
Rigopoulou, D., Lawrence, A., & Rowan-Robinson, M. 1996, MNRAS, 278, 1049
Roseboom, I. G., Dunlop, J. S., Cirasuolo, M., et al. 2013, MNRAS, 436, 430
Skelton, R., Whitaker, K. E., Momcheva, I. G., et al. 2014, ApJS, 214, 24
Smail, I., Ivison, R. J., & Blain, A. W. 1997, ApJL, 490, L5
Strandet, M. L., Weiß, A., Vieira, J. D., et al. 2016, ApJ, 822, 80
Wang, W.-H., Cowie, L. L., Barger, A. J., & Williams, J. P. 2011, ApJL,726, L18
Wang, W.-H., Lin, W.-C., Lim, C.-F., et al. 2017, ApJ, 850, 37

Younger, J. D., Fazio, G. G., Wilner, D. J., et al. 2008, ApJ, 688, 59